DOI: 10.21062/mft.2025.056 © 2025 Manufacturing Technology. All rights reserved. http://www.journalmt.com

Experimental Evaluation of Vibration Responses to Progressive Gear Damage in Planetary Gear

Tomáš Gajdošík (0000-0002-0622-2427), Matúš Vereš (0009-0005-9469-3016), Igor Gajdáč (0000-0002-1315-2914), Ronald Bašťovanský (0000-0002-1551-2346)

Faculty of Mechanical Engineering, University of Žilina in Žilina. Univerzitná 8215/1, 010 26 Žilina. Slovak Republic.

This study presents a systematic experimental analysis of vibration responses in a planetary gearbox (type A2000) under both undamaged and artificially induced fault conditions. The primary aim was to identify specific frequency-domain signatures of various types and severities of gear defects—such as pitting on the flanks of gear teeth, missing teeth, unbalance of the carrier, and damage to the ring gear—through spectral analysis of vibration signals. Measurements were conducted in both loaded and unloaded states using non-contact torque sensors and a multi-channel diagnostic system (SKF IMx-S) with tri-axial accelerometers. The results demonstrate a strong correlation between the severity of gear damage and the amplitude and structure of sidebands around the gear mesh frequencies. Notably, the presence of pitting consistently increased the sideband amplitudes, while unbalance induced distinct harmonics in the frequency spectrum. Damage to the ring gear and central gear exhibited overlapping features but were distinguishable in the acceleration envelope spectrum. The findings provide a foundation for the early-stage identification of gearbox faults and highlight the potential for deploying automated diagnostic systems in industrial applications. Future work will focus on real-time AI-based detection methods and application of the results in industrial environments such as Continental and U.S. Steel.

Keywords: Gearbox diagnostics, Planetary gearbox, Vibration analysis, Gear damage detection, Artificial damage on gears

1 Introduction

Vibration-based diagnostics is central to predictive maintenance, enabling non-invasive, early detection of degradation. As assets face higher loads, variable speeds, and complex duty cycles, classic time-/frequency-domain tools are complemented by time-frequency methods, statistical indicators, machine learning, and hybrid signal-AI systems [1-10]. These approaches expose incipient bearing/gear faults, cutting downtime and improving safety and asset life [1, 4, 11, 12]. Multisensor fusion (vibration + acoustic/thermal/electrical) improves robustness [1, 12, 13], while SVMs, neural networks, and federated learning enable real-time diagnosis under variable conditions [1-4, 7], reinforcing vibration analysis in modern PHM [1, 2, 5].

Continuous industries near design limits need early fault identification for turbines, pumps, compressors, and large gearboxes; sound monitoring reduces unplanned downtime, increases availability, and aligns maintenance with true condition [1, 2, 5, 14]. Gearbox failures carry high consequences [7-10, 13, 15], with reports up to 38% of failures tied to gearboxes in metallurgy [14] and maintenance reaching ~50% of production costs [1]. Data-driven vibration+AI raises detection accuracy, shortens response, and cuts costs by tens of percent [2, 16].

Planetary gearboxes offer high power density, compactness, large ratios, and even load sharing [15, 17-19], suiting wind and aerospace applications [20-24]. Diagnostics are difficult: multiple meshes and moving frames yield modulated, crowded spectra with overlapping sidebands [21, 23, 25-29]; resonances, symmetry, and path variability hinder localization/classification [15, 20, 24, 30]. Thus, order tracking, time—frequency analysis, and resonance-based extraction are often required, especially at variable speed/load [15, 18, 24, 29, 31-33].

Common gear faults include pitting, tooth breakage, wear, eccentricity, axial carrier imbalance, and bearing damage. Pitting alters mesh stiffness and adds harmonics [28, 34-37]; tooth breakage induces impulsive/non-harmonic content [32, 35, 38-40]; reduced stiffness modulates harmonics around GMF [30, 35, 36]. Complementary indicators include thermal, acoustic, and spectral statistics [28, 32-34, 37, 41, 42]. Diagnostics therefore track GMF, its harmonics, and GMF-centred sidebands from periodic deviations/faults [16, 28, 30, 34, 35]. GMF (tooth count × rotational frequency) is highly sensitive; sidebands near GMF/multiples reflect periodic stiffness variation or imbalance [10, 16, 28, 38, 40]. Additional components tied to shaft speeds often accompany eccentricity or bearing faults. Integrated vibrationacoustic-thermal monitoring is increasingly advocated, including digital-twin use cases [23, 41].

Although model-based diagnostics—digital twins and numerical simulations—are gaining traction [30, 35, 30, 43, 44], they rely on idealised representations and estimated fault parameters. Their direct transferability to complex planetary systems can be limited, particularly for subtle or interacting faults. Some studies address this by deliberately inducing mechanical damage in the laboratory to observe fault-specific spectral features under controlled conditions [7, 29, 32-34, 36, 38, 39, 45-50], yet such work remains comparatively scarce for planetary transmissions.

Against this backdrop, the present study adopts a fully experimental approach: systematically creating known faults in selected components of a planetary gearbox and characterising their frequency-domain vibration response, with emphasis on the spectral manifestation and severity of each mode. The goal is to support diagnostic frameworks for planetary gearboxes in continuous-duty operation. Results will be directly applied in condition monitoring at Continental Púchov and U.S. Steel Košice, helping bridge the gap between experimental validation and real-world implementation.

2 Materials and Methods

2.1 Test Rig

To support vibration-based diagnostics of planetary gearboxes, a dedicated test rig was constructed at the Department of Design and Machine Elements, University of Žilina. The system was designed specifically for experimental analysis of gear fault signatures under controlled conditions, and it featured two A2000 planetary gearboxes connected in series to enable symmetrical load distribution and facilitate fault isolation.

As shown in Figure 1, the test rig consisted of a 2-pole asynchronous motor (ABB M2QA 160M2B) rated at 15 kW, operating at 440 V and 60 Hz, and controlled via an ABB frequency inverter. The motor was followed by the first A2000 planetary gearbox, which was directly connected to a second identical gearbox. These were mounted in opposing configurations, resulting in an overall gear ratio of 1:1. A dynamometer was placed at the end of the drivetrain to provide loading conditions and to close the power loop.

Torque transmission between components was achieved using DIN-standard joint shafts. The connection between the motor and the first gearbox, as well as between the second gearbox and the dynamometer, used DIN 150 shafts. A larger DIN 200 joint shaft was employed to connect the two planetary gearboxes.

For measurement purposes, two non-contact torque and rotational speed sensors (HBM T10F) were installed—one on the motor output shaft and the other on the input shaft of the first gearbox stage. The placement of both sensors is highlighted in Figure 1.



Fig. 1 Test rig assembled in the laboratory of the Department of Design and Machine Elements, University of Zilina; a – final assembly of test rig; b – test rig with highlighted sensor positions

The tested gearbox, type A2000 (as well as the reduction gearbox), is a double-stage planetary gearbox featuring straight involute gearing. The kinematic arrangement of the gearbox configuration within the test rig is illustrated in Figure 2. The basic technical parameters of the A2000 gearbox are summarised in Table 1.

Prior to initial measurements, both A2000 gearboxes were fully disassembled, cleaned, and subjected to a comprehensive technical inspection. As part of this process, seals and other necessary components were replaced. After reassembly, the gearboxes were mounted into dedicated frames and installed into their designated positions within the test rig.

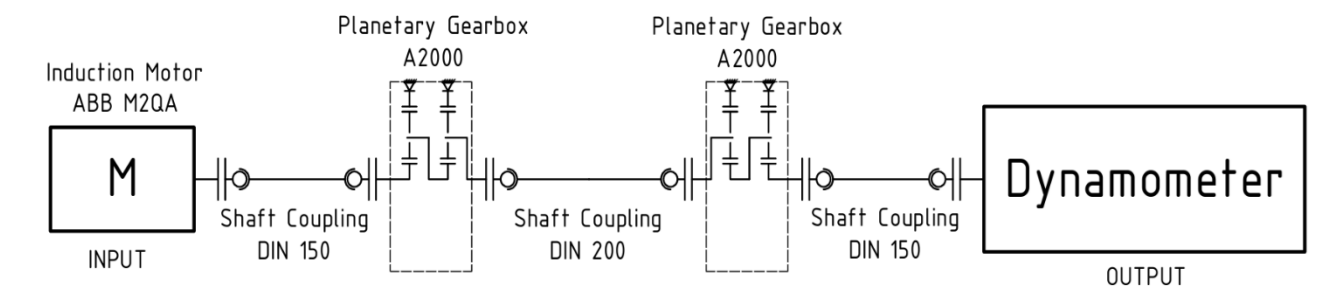


Fig. 2 Kinetic diagram of test rig

Tab. 1 Technical Parameters of A2000 Gearbox

Parameter	1st Stage	2 nd Stage	
Number of Sun Gear Teeth	40	23	
Number of Ring Gear Teeth	116	97	
Number of Planet Gear Teeth	37	36	
Gear Ration i _{1,2}	3.90	5.217	
Internal Gear Ratio u _{v1,2}	-2.9	-4.217	
Number of Planet Gears λ _s	3	3	
Gear Module m _{1,2}	3	3.5	
Total Transmission Ratio ic	20.348		

2.2 Diagnostic Equipment



Fig. 3 Mounting of vibration sensors on the housing of the tested A2000 gearbox; Directions: x - axial; y - tangential; z - radial

The diagnostic instrumentation consisted of an SKF IMx-S data acquisition system used for continuous signal monitoring. Vibration signals were captured using an array of six accelerometers—three mounted on each gearbox—measuring vibrations in the axial (x), tangential (y), and radial (z) directions. All sensors had a sensitivity of 100 mV/g (SKF), as illustrated in Figure 3. Rotational speed was measured

using a laser tachometer probe. Once the measurement system was connected to a PC, the recorded data could be managed, visualised, exported, and analysed using the SKF @ptitude Analyst software. The sampling rate used for the measurements was set to 3200 lines of resolution.

2.3 Measurement Conditions

The tested A2000 gearbox operated at a constant input speed of 1470 ± 10 RPM. Depending on the testing scenario, the input shaft rotation could be set in either the clockwise or counterclockwise direction. During unloaded measurements, the applied torque was set to 15 Nm, which corresponded to the internal losses of the entire test rig. Under loaded conditions, the gearbox was subjected to an input torque of 42 Nm.

2.4 Calculation of Characteristic Frequencies

To enable the identification of specific gearbox components—such as bearings and gear meshes—in the frequency spectrum, it was first necessary to calculate their characteristic frequencies based on the input rotational speed. These calculations were performed in Microsoft Excel using standard equations, ensuring that all resulting frequencies were referenced to the input speed of the A2000 gearbox. The calculated frequency values are summarised in Table 2.

Tab. 2 Characteristics frequencies of the A2000 planetary gearbox

Input speed [RPM]	1470.00		
Output speed [RPM]	1470.00		
	Angular Velocities [rad.s-1]		
Component	1st Stage	2nd Stage	
Sun Gear	153.938	39.471	
Carrier	39.471	7.565	
Planet Gear	-123.748	-20.384	
Ring Gear	0	0	
	Speeds [RPM]		
Component	1st Stage	2nd Stage	
Sun Gear	1470.00	376.923	
Carrier	376.923	72.244	
Planet Gear	-1181.705	-194.656	
Ring Gear	0	0	
	Speeds [Hz]		
Component	1st Stage	2nd Stage	
Sun Gear	24.5	6.282	
Carrier	6.282	1.204	
Planet Gear	19.695	3.244	
Ring Gear	0	0	
	Meshing Frequencies [Hz]		
Frequency Description	1st Stage	2nd Stage	
Meshing freq. sun-planet	728.718	116.794	
Meshing freq. ring-planet	728.718	116.794	
Tooth freq. of sun gear	54.654	15.234	
Tooth freq. of planet gear	39.390	6.489	
Tooth freq. of ring gear	18.846	3.612	

2.5 Experimental Procedure

The experimental procedure began with baseline data acquisition from both undamaged gearboxes, which were filled with the prescribed volume of lubricant and operated under both unloaded and loaded conditions. The collected vibration data were subjected to detailed spectral analysis to identify the characteristic frequencies of individual gearbox components. Based on this analysis, one gearbox was selected for the subsequent phase of testing, during which

controlled damage would be systematically introduced into specific components.

The initial spectral comparison showed that signals captured in the x (axial), y (tangential), and z (radial) directions exhibited similar frequency structures, differing mainly in amplitude. Since the z-axis spectra consistently displayed the most pronounced amplitude responses for critical frequencies, all subsequent measurements were limited to the radial direction to improve signal clarity and measurement efficiency.

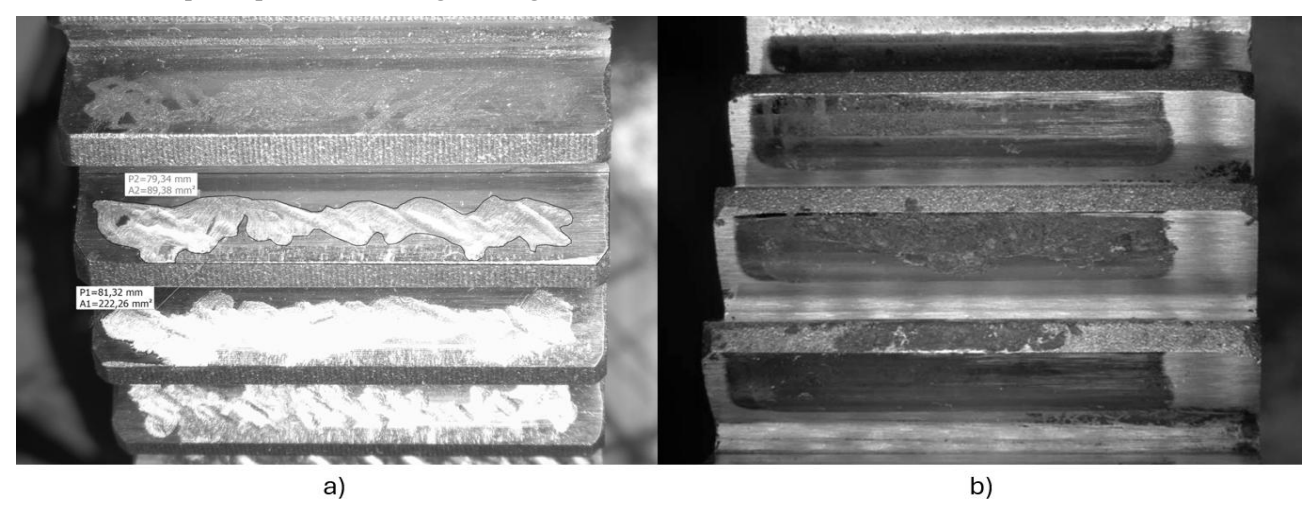


Fig. 4 Pitting damage on approximately half of the teeth of the sun gear (a); Pitting damage on all teeth of the sun gear (b)

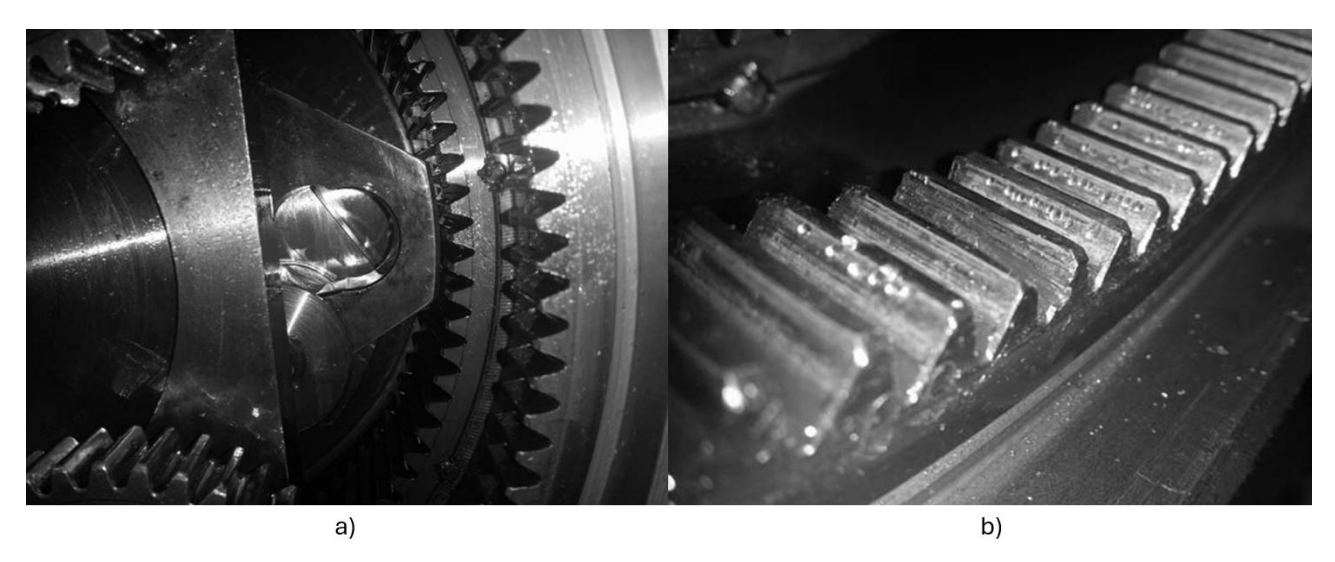


Fig. 5 Detail of the carrier with a drilled hole causing imbalance (a); Ring gear with pitting damage on multiple teeth (b)

After completing the reference measurements, the first damage-response testing phase began. In this phase, progressive damage was introduced into the sun gear of the first planetary stage. Vibration data were collected to assess the spectral manifestation of each defect. The damage scenarios applied to the sun gear followed this sequence:

- Localised pitting on the flank of a single tooth
- Pitting on approximately half of the gear teeth (Figure 4a).
- Pitting on the flank of every tooth of the sun gear (Figure 4b).

In the second phase of testing, vibration data were collected from a single-stage A2000 planetary gearbox. During this stage, damage was introduced to the ring

gear. Throughout all measurements in this phase, the system also included a constant defect in the form of carrier imbalance. This imbalance was artificially created by drilling a hole approximately 30 mm in diameter into the carrier body. The test sequence was as follows:

- Pitting on the flank of all sun gear teeth combined with the removal of one sun gear tooth, along with the carrier imbalance (Figure 5a).
- Pitting on the flanks of several teeth of the ring gear (Figure 5b), with the carrier imbalance remaining present.

3 Results and Discussion

Table 3 summarises the individual measurement stages and specifies the corresponding test conditions.

Tab. 3 Fault Sets

Baseline Measurements							
Test Type	Damaged Compo- nent	Fault Type	Fault Severity	Gearbox Load [N.m]			
Unloaded Test	No Damage	No Damage	-	15			
Loaded Test	No Damage	No Damage	-	42			
First Measurement Stage							
Test Type	Damaged Compo- nent	Fault Type	Fault Severity	Gearbox Load [N.m]			
Pitting on One Tooth Flank	Sun Gear	Pitting	One Tooth Damaged	42			
Pitting on Half of the Teeth	Sun Gear	Pitting	Half of the Teeth Damaged	42			
Pitting on All Teeth	Sun Gear	Pitting	All Teeth Damaged	42			
Second Measurement Stage							
Test Type	Damaged Compo- nent	Fault Type	Fault Severity	Gearbox Load [N.m]			
Pitting on All Teeth + Carrier Imbalance	Sun Gear / Carrier	Pitting, Missing To- oth / Carrier Imba- lance	All Teeth Damaged / One Missing Tooth / Hole with 30mm Diameter	42			
Ring Gear Damage	Ring Gear / Carrier	Pitting / Carrier Im- balance	18 Teeth Damaged / Hole with 30mm Diameter	42			

3.1 Baseline Measurements

The baseline tests included measurements of an undamaged gearbox operating under both unloaded and loaded conditions. The first unloaded run served primarily to familiarise with the test rig and to obtain reference data used to identify the characteristic frequencies of gearbox components in the spectral domain.

Figure 6 shows a detailed view of the vibration velocity spectrum in the Z direction for the unloaded,

undamaged gearbox. Highlighted in the spectrum are the output shaft frequency $f_{OTx} = 1.25 \, Hz$ (yellow), the input shaft frequency $f_{OTa} = 24.69 \, Hz$ (light blue), the mesh frequency of the first planetary stage $f_{zl} = 725.3 \, Hz$ (dark blue), and the mesh frequency of the second planetary stage $f_{zl} = 115.6 \, Hz$ (red). The spectrum is dominated by f_{zl} with its second $2f_{zl}$, third $3f_{zl}$, and fourth $4f_{zl}$, harmonics clearly visible. In addition, the second harmonic of the first-stage mesh frequency $2f_{zl}$ also appears in the spectrum.

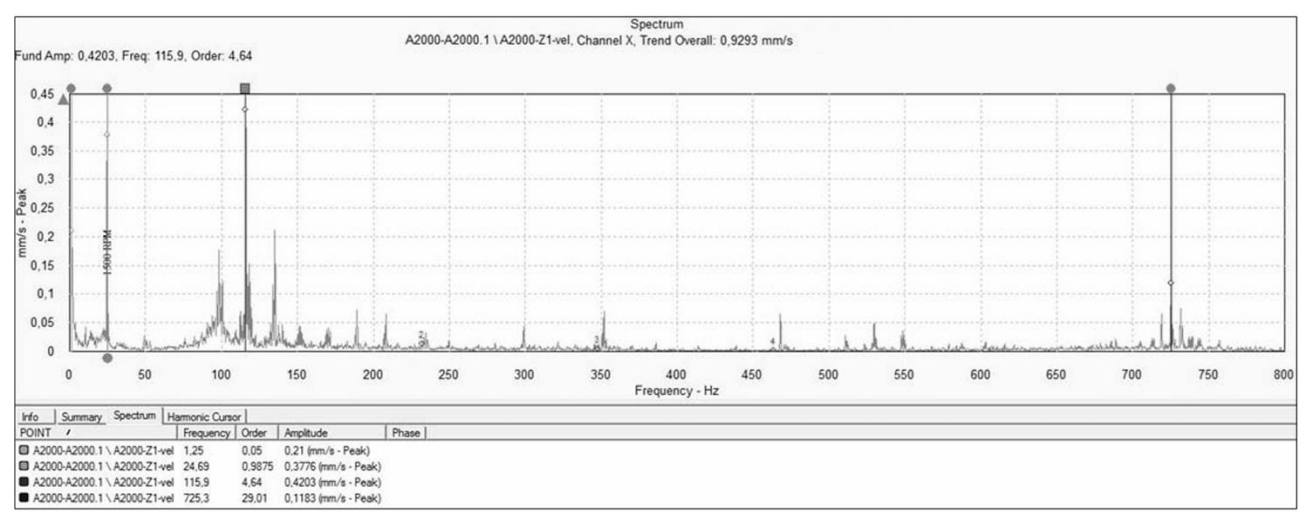


Fig. 6 Vibration velocity spectrum in the Z-direction for undamaged, unloaded gearbox

Figure 7 presents a waterfall plot comparing the frequency spectra of vibration velocity in the Z direction for the unloaded (top) and loaded (bottom) gearbox states. The red horizontal line separating the two spectra indicates the shutdown of the test rig between measurements.

The comparison reveals a noticeable increase in the amplitudes of the output shaft frequency f_{OTx} , input

shaft frequency f_{OTa} , and the mesh frequency of the first planetary stage $f_{\chi l}$ under load. While the shape of the sideband structure around the second-stage mesh frequency $f_{\chi l}$ remains largely unchanged, the sidebands around $f_{\chi l}$ exhibit a significant asymmetry. In particular, the amplitude of the right-side components adjacent to $f_{\chi l}$ decreases considerably under load.

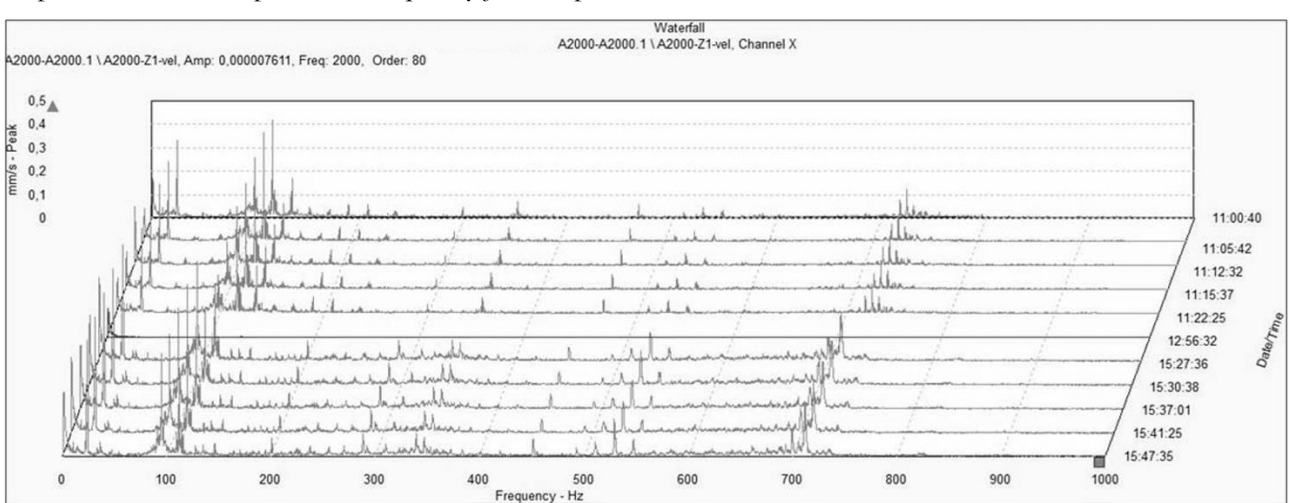


Fig. 7 Waterfall plot comparing vibration velocity spectra in the Z-direction: unloaded gearbox (top) vs. loaded gearbox (bottom)

3.2 First Measurement Stage

The results obtained during the first stage of testing yielded the following key observations:

 In the presence of pitting damage on the flank of a single tooth, an increase in the amplitude of the sidebands around the corresponding

- gear mesh frequency is observed in the vibration velocity spectrum. The sideband amplitude grows proportionally with the extent of damage, while the amplitude of the fundamental gear mesh frequency remains nearly unchanged.
- As pitting extends to multiple teeth, the second harmonic of the mesh frequency begins to emerge in the spectrum, with the third harmonic also becoming discernible (Figure 8).
- When the pitting area spreads to more than half of the gear teeth, a sideband structure begins to form around the mesh frequency with a spacing equal to the tooth passing frequency of the damaged sun gear. Initially, this sideband is weak. However, as pitting progresses to all teeth, the sideband becomes more pronounced (Figure 9). In this advanced state, the second and third harmonics of the mesh frequency become clearly visible, and the fourth harmonic begins to appear (Figure 8).

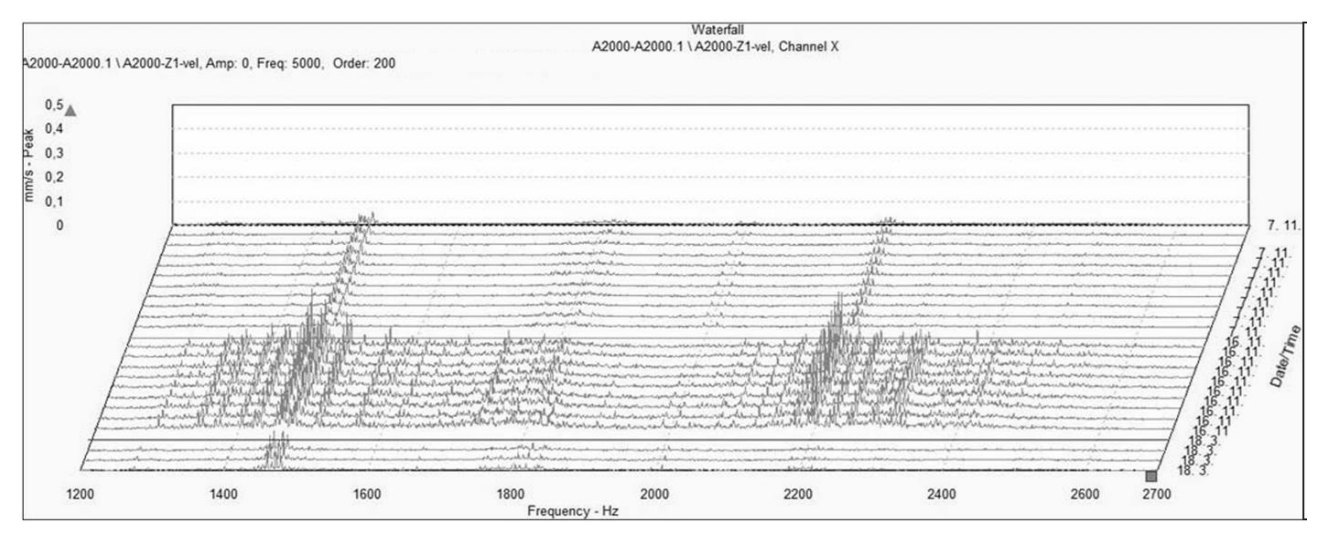


Fig. 8 Comparison of vibration velocity spectra for the sun gear with pitting on one tooth (top), on all teeth (middle), and on half of the teeth (bottom) — detail 1

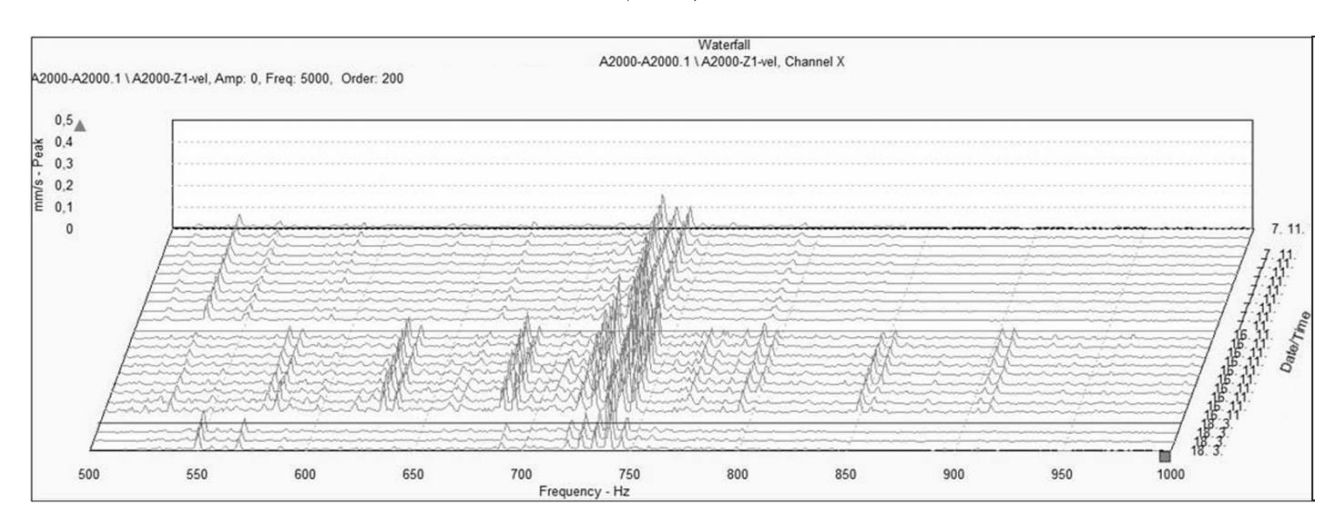


Fig. 9 Comparison of vibration velocity spectra for the sun gear with pitting on one tooth (top), on all teeth (middle), and on half of the teeth (bottom) — detail 2

In the acceleration envelope spectrum filtered by Band 3, the following patterns were observed:

• When pitting damage affects the flank of a single tooth, the spectrum reveals the tooth meshing frequency of the damaged gear and its harmonics. Around this tooth frequency, a

sideband structure emerges with a spacing corresponding to the rotational frequency of the affected gear (Figures 10 and 11). This spectral pattern remains consistent as the damage expands; only the amplitude of the tooth frequency and its harmonics increases.

 The highest amplitude values were recorded in the case of damage affecting all teeth. Compared to the condition with only one tooth affected, the tooth frequency amplitude increased by nearly 2100%. However, this value strongly depends on the total area of the pitted surface [28, 41, 43]; in our case, the average pitting coverage reached approximately 55% of the total flank surface (Figure 11).

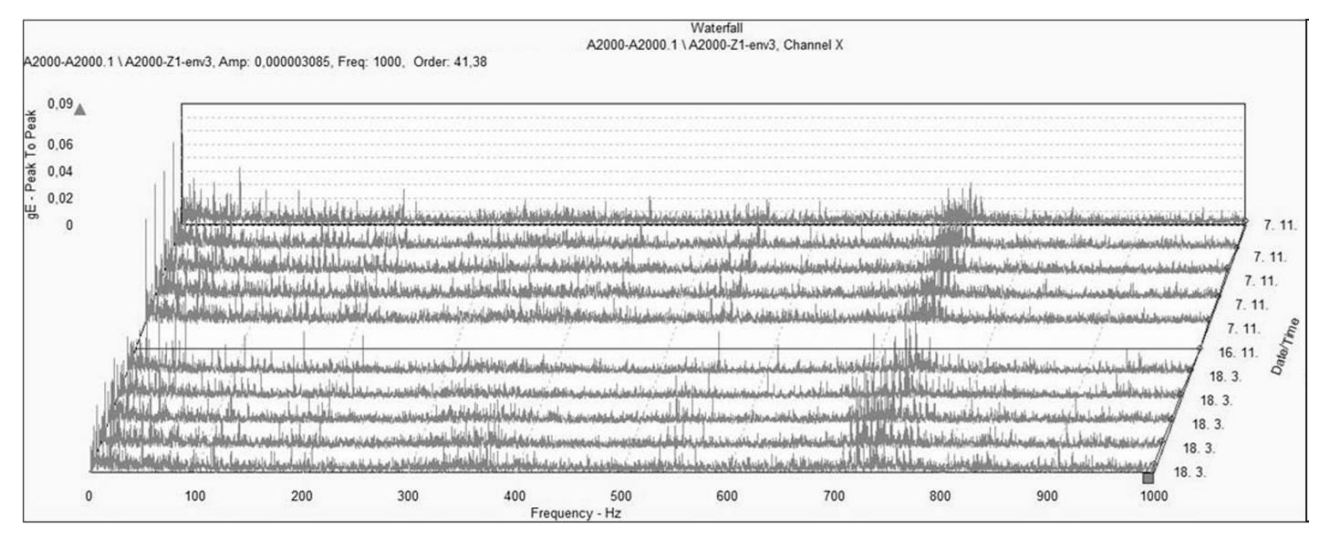


Fig. 10 Comparison of acceleration envelope spectra (filter 3) for the sun gear with pitting on one tooth (top) and on half of the teeth (bottom)

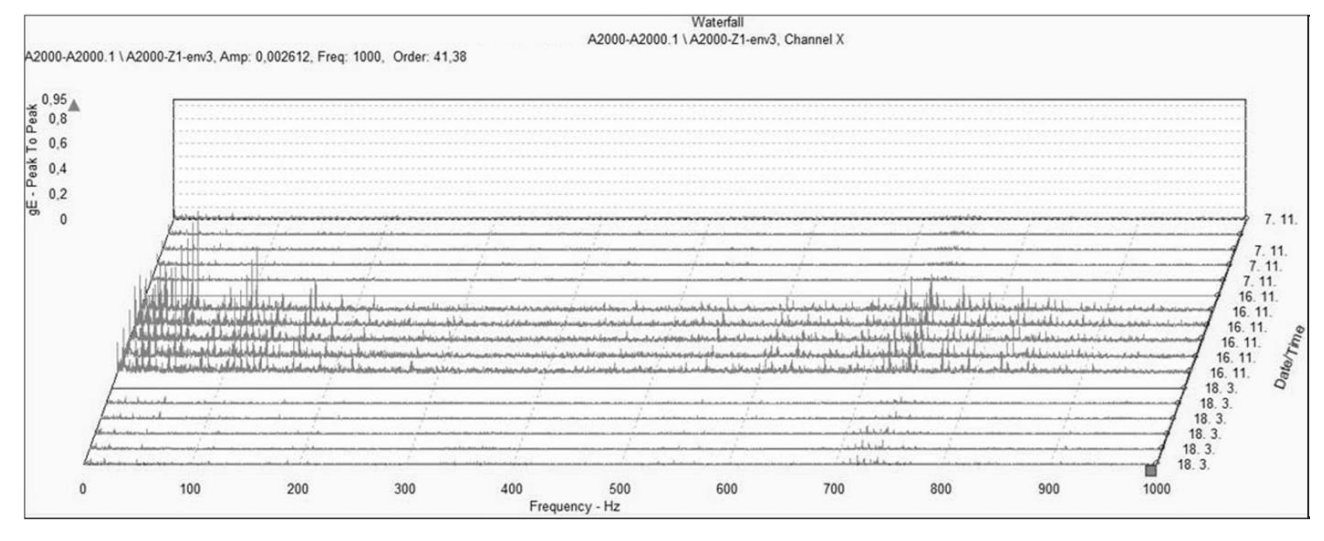


Fig. 11 Comparison of acceleration envelope spectra (filter 3) for the sun gear with pitting on one tooth (top), on all teeth (middle), and on half of the teeth (bottom)

3.3 Second Phase of Measurements

The analysis of the data collected during the second phase of testing led to the following conclusions:

- The spectral response of the central gear with pitting on all tooth flanks was consistent under both loaded and unloaded conditions. The mesh frequency of the affected planetary stage became more prominent, accompanied by stronger second and third harmonics, and in cases of severe damage, also the fourth harmonic. An additional sideband appeared
- around the mesh frequency, with spacing equal to the tooth frequency of the damaged central gear (Figure 12).
- The imbalance of the carrier manifested as an increase in the amplitude of its rotational frequency. This was surrounded by a pronounced sideband structure, where the first and second sideband components were clearly visible. The spacing of this sideband was approximately one-tenth of the carrier's rotational frequency.

• Damage to the ring gear exhibited spectral behaviour similar to that of the central gear. It was most clearly observed in the acceleration envelope spectrum (Filter 3), where the spectrum was dominated by the ring gear tooth frequency and its harmonics, which extended across nearly the entire spectral range (Figure 13).

Figure 12 displays three vibration velocity spectra:

• The top spectrum corresponds to a gearbox with severe central gear damage (tooth removed and pitting on all teeth).

- The middle spectrum shows moderate pitting on approximately half the teeth.
- The bottom spectrum was recorded with both minor pitting on the central gear and additional damage to the ring gear.

As can be seen in Figure 12, the most significant spectral response occurred when all central gear teeth were affected by pitting and one tooth was removed. In contrast, the spectral signature of the ring gear damage was nearly indistinguishable in this comparison.

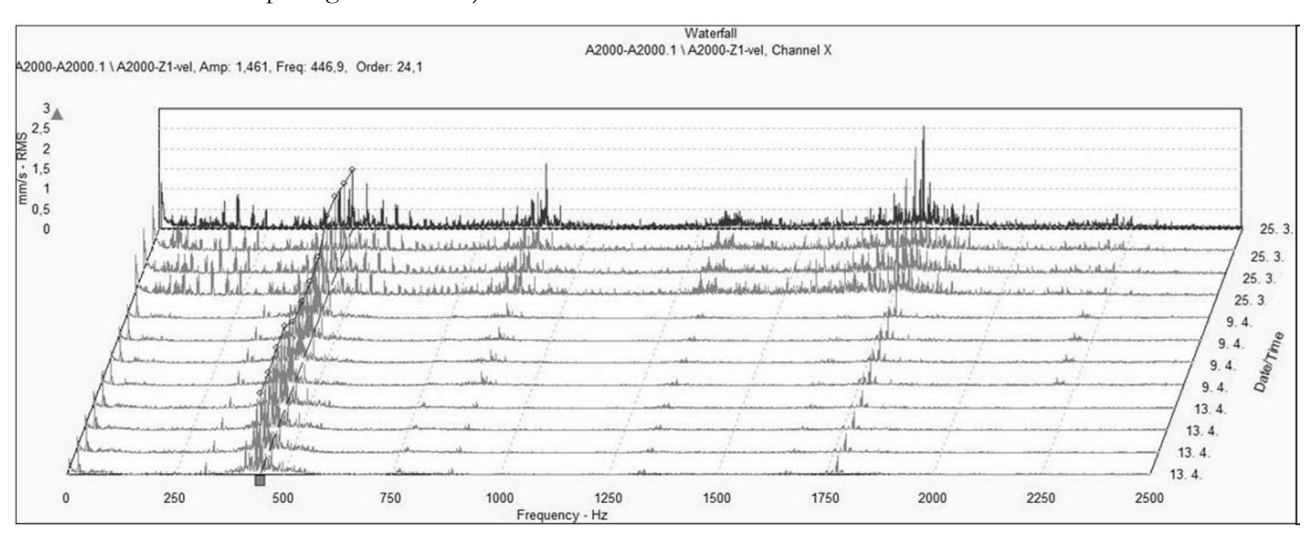


Fig. 12 Comparison of vibration velocity spectra during the second measurement stage: gearbox with a missing tooth on the sun gear (top), gearbox with moderate pitting (middle), and gearbox with ring gear damage (bottom)

In the acceleration envelope spectra using Filter 3 (Figure 13), the top section illustrates the response of a central gear exhibiting pitting and a missing tooth. The spectrum is dominated by the tooth frequency of the damaged gear and its harmonics. In the middle section, a significant decrease in vibration amplitudes is observed after replacing the central gear with one

affected only by pitting on approximately half of the teeth. The bottom section presents the spectral response to damage on the ring gear, which again manifests as elevated amplitudes at the central gear tooth frequency and its harmonics - visible up to roughly the midpoint of the measured frequency range.

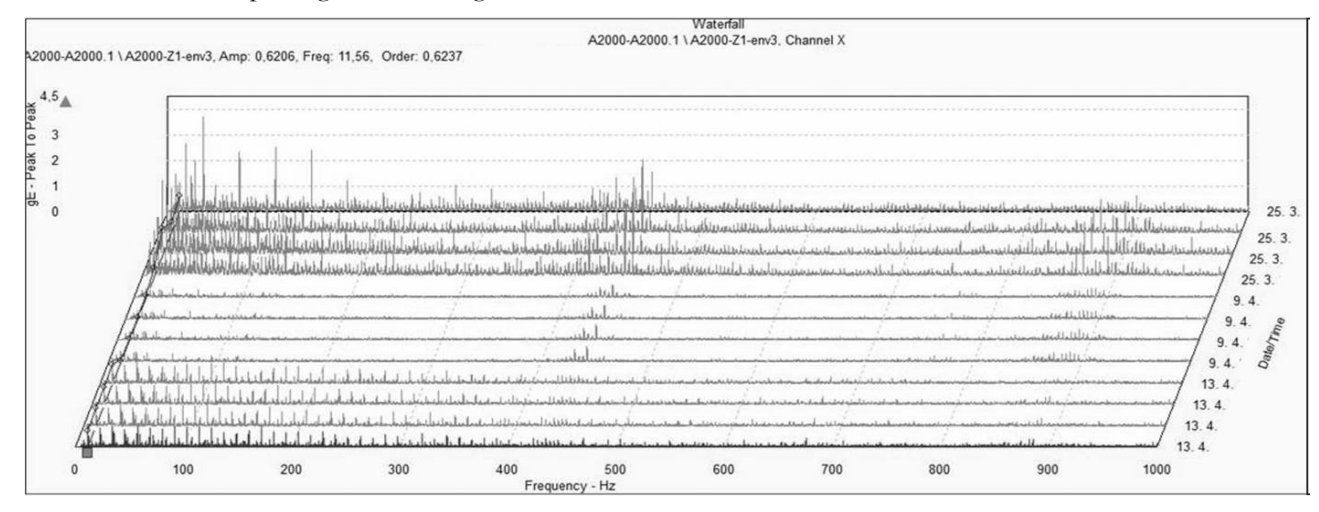


Fig. 13 Comparison of acceleration envelope spectra (filter 3) during the second measurement stage: gearbox with a missing tooth on the sun gear (top), gearbox with moderate pitting (middle), and gearbox with ring gear damage (bottom)

3.4 Summary of Results and Discussion

The experimental data demonstrate that pitting on the flank of a single tooth of the central gear leads to a noticeable increase in the amplitudes of sidebands surrounding the corresponding gear mesh frequency (GMF) in the vibration velocity spectrum. As the severity of the damage increases, the sideband amplitudes grow accordingly, while the amplitude of the GMF itself remains nearly constant.

When the pitting extends to more than half of the teeth, a sideband pattern begins to emerge around the GMF, with spacing corresponding to the tooth passing frequency of the damaged gear. Although initially subtle, the second harmonic of the GMF becomes evident, followed by weak traces of the third harmonic. Once the damage encompasses all gear teeth, the sideband becomes significantly more pronounced, and the second and third harmonics are clearly visible. At this stage, the fourth harmonic also starts to emerge.

The imbalance of the planetary carrier manifests as a substantial increase in the amplitude of its rotational frequency, accompanied by a distinct sideband structure. The spacing of this sideband is approximately one-tenth of the carrier frequency, and both the first and second-order components are clearly detectable.

Damage to the ring gear exhibits spectral behaviour similar to that of the central gear. The most distinct representation is found in the acceleration envelope spectrum (Filter 3), where the tooth passing frequency of the ring gear and its harmonics dominate nearly the entire spectrum.

Looking forward, the acquired knowledge is intended to be applied in industrial settings, specifically at Continental Púchov and U.S. Steel Košice. Moreover, the implementation of artificial intelligence and machine learning algorithms for real-time condition monitoring is envisioned. These advanced systems could enable early detection of gearbox faults—such as the onset of pitting—before they progress into irreversible damage, including tooth breakage. This would not only prevent unplanned outages and potential catastrophic failures but could also significantly reduce the costs associated with maintenance and diagnostics [2, 16].

4 Conclusion

The current findings confirm that distinct fault signatures of individual gearbox components can be reliably identified within the vibration frequency spectrum. However, accurate detection depends on the application of appropriate diagnostic methods and spectral evaluation techniques. The laboratory measurements provide detailed insight into the characteristic frequency responses of specific faults, which can subsequently be compared with field data from

operational machinery to assess gearbox condition more precisely.

Ongoing experimental work aims to expand the fault database by introducing additional types of damage—particularly on the ring gear and potentially also in bearing components—to further refine the diagnostic framework. These extended measurements will help build a more comprehensive understanding of failure modes and their spectral manifestations.

The results are intended primarily to support industrial diagnostics in facilities such as Continental Púchov and U.S. Steel Košice. In addition, the measured datasets could form the foundation for developing an automated diagnostic system for continuous gearbox condition monitoring, in line with recent trends in the literature [2, 14, 41].

Acknowledgement

This work was supported by the Scientific Grant Agency of the Ministry of Education, Science, Research and Sport of the Slovak Republic (VEGA), project no. 1/0568/24, Research in the field of loading and stress deformation states of rolling bearing cages. The authors gratefully acknowledge this support.

References

- [1] ROMANSSINI, M., DE AGUIRRE, P. C. C., COMPASSI-SEVERO, L., GIRARDI, A. G. (2023). A review on vibration monitoring techniques for predictive maintenance of rotating machinery. In: *Eng*, Vol. 4, No. 3, pp. 1797-1817.
- [2] KESHTA, I., MAJEED, M. E., AL-SHAIKHLI, T. R., ADEL, A. H., JABBAR, K. A., SONI, M. (2025). AI-Based Predictive Maintenance for Machine Vibration and Condition Monitoring in Industrial Applications. In: 2025 4th OPJU International Technology Conference (OTCON) on Smart Computing for Innovation and Advancement in Industry 5.0, pp. 1-7. IEEE.
- [3] CÉZOVÁ, E. (2025). Demonstration of Neural Network in Prediction of Bearing Lifetime. In: *Manufacturing Technology Journal*, Vol. 25, No. 2, pp. 170-173. Elsevier.
- [4] BOUZOUIDJA, M., SOUALHI, M., SOUALHI, A., RAZIK, H. (2024). Detection and diagnostics of bearing and gear fault under variable speed and load conditions using heterogeneous signals. In: *Energies*, Vol. 17, No. 3, p. 643. MDPI.
- [5] SAIED, R. O., MOSTAFA, M. S., HUSSEIN, H. A. (2015). Predictive maintenance program based on vibration monitoring. In: *Design and*

- Modeling of Mechanical Systems-II: Proceedings of the Sixth Conference on Design and Modeling of Mechanical Systems, CMSM'2015, March 23-25, Hammamet, Tunisia, pp. 651-660. Cham: Springer International Publishing.
- [6] DU, Y., LU, Z., CHANG, E., LI, Q., SHI, Y. (2023). Identification Method of Vibration Drilling Bit Wear State Based on Signal Imaging and Deep Learning. In: *Manufacturing Technology Journal*, Vol. 23, No. 4, pp. 392-398. Elsevier.
- [7] DUBAISH, A. A., JABER, A. A. (2023). Fabrication of a test rig for gearbox fault simulation and diagnosis. In: *Diagnostyka*, Vol. 24
- [8] AHERWAR, A. (2012). An investigation on gearbox fault detection using vibration analysis techniques: A review. In: Australian Journal of Mechanical Engineering, Vol. 10, No. 2, pp. 169-183. Taylor & Francis.
- [9] PECHO, P., HRÚZ, M., NOVÁK, A., TRŠKO, L. (2021). Internal damage detection of composite structures using passive RFID tag antenna deformation method: Basic research. In: Sensors, Vol. 21, No. 24, p. 8236. MDPI.
- [10] ZUBER, N., BAJRIĆ, R., ŠOSTAKOV, R. (2014). Gearbox faults identification using vibration signal analysis and artificial intelligence methods. In: *Eksploatacja i Niezawodność*, Vol. 16, No. 1, pp. 61-65.
- [11] LI, Q., CAI, X., LI, W., TAN, Z., YANG, C. (2023). Progress and Prospect of Ultrasonic Vibratory Cutting Research. In: *Manufacturing Technology Journal*, Vol. 23, No. 5, pp. 638-648. Elsevier.
- [12] QU, Y., HE, D., YOON, J., VAN HECKE, B., BECHHOEFER, E., ZHU, J. (2014). Gearbox tooth cut fault diagnostics using acoustic emission and vibration sensors-A comparative study. In: *Sensors*, Vol. 14, No. 1, pp. 1372-1393. MDPI.
- [13] GOSWAMI, P., RAI, R. N. (2024). Principal component analysis based vibration sensor selection for fault diagnosis of an industrial gearbox. In: 2024 IEEE International Instrumentation and Measurement Technology Conference (I2MTC), pp. 1-6. IEEE.
- [14] SEO, M. K., YUN, W. Y. (2024). Gearbox Condition Monitoring and Diagnosis of Unlabeled Vibration Signals Using a Supervised Learning Classifier. In: *Machines*, Vol. 12, No. 2, p. 127. MDPI.

- [15] HILBERT, M., SMITH, W. A., RANDALL, R. B. (2022). The effect of signal propagation delay on the measured vibration in planetary gearboxes. In: *Journal of Dynamics, Monitoring and Diagnostics*, Vol. 1, No. 1, pp. 9-18.
- [16] JIN, X., CHENG, F., PENG, Y., QIAO, W., QU, L. (2018). Drivetrain gearbox fault diagnosis: Vibration-and current-based approaches. In: IEEE Industry Applications Magazine, Vol. 24, No. 6, pp. 56-66. IEEE.
- [17] CHOY, F. K., HUANG, S., ZAKRAJSEK, J. J., HANDSCHUH, R. F., TOWNSEND, D. P. (1996). Vibration signature analysis of a faulted gear transmission system. In: *Journal of Propulsion and Power*, Vol. 12, No. 2, pp. 289-295.
- [18] ZOU, M., MA, J., XIONG, X., LI, R. (2023). Analysis of vibration characteristics of planetary gearbox with broken sun gear based on phenomenological model. In: *Applied Sciences*, Vol. 13, No. 16, p. 9413. MDPI.
- [19] KOHÁR, R., HRČEK, S., BRUMERČÍK, F. (2021). The comparison of the amount of backlash of a harmonic gear system. In: *Tehnički vjesnik*, Vol. 28, No. 3, pp. 771-778.
- [20] LIU, L., ZUO, M. J., LIANG, X. (2016). Dependence analysis of planetary gearbox vibration marginals. In: 2016 Prognostics and System Health Management Conference (PHM-Chengdu), pp. 1-6. IEEE.
- [21] MIAO, Q., ZHOU, Q. (2015). Planetary gearbox vibration signal characteristics analysis and fault diagnosis. In: *Shock and Vibration*, Vol. 2015, p. 126489. Wiley.
- [22] HEMATI, A., SHOOSHTARI, A. (2025). Planetary Gearbox Vibration Analysis Using Experimental Validation and Dynamic Simulation. In: *Journal of Vibration Engineering & Technologies*, Vol. 13, No. 4, p. 232. Springer Nature.
- [23] YU, X., FENG, Z., LIANG, M. (2021). Analytical vibration signal model and signature analysis in resonance region for planetary gearbox fault diagnosis. In: *Journal of Sound and Vibration*, Vol. 498, p. 115962. Elsevier.
- [24] MIRONOV, A., MIRONOVS, D. (2018). Vibration diagnostics of planetary gearbox of engineering and transport machines based on spatial model application. In: 17th International Scientific Conference Engineering for Rural Development, pp. 23-25.
- [25] SÁSIK, R., BAŠŤOVANSKÝ, R., HOČ, M., MADAJ, R., SPIŠÁK, P. (2019). The comparison of selected strength indicators of

- manufactured prototypes produced by metal additive manufacturing (3D printing) system. In: *Current Methods of Construction Design: Proceedings of the ICMD 2018*, pp. 501-508. Cham: Springer International Publishing.
- [26] OSMAN, A., GOBRAN, M. H., MAHMOUD, F. F. (2020). Vibration Signature of Gear Pump of Missing One and Two Teeth. In: The Egyptian International Journal of Engineering Sciences and Technology, Vol. 30, pp. 39-50.
- [27] CHARDE, M.M., NAJAN, T.P., CEPOVA, L., JADHAV, A.D., RASH-INKARD, N.S., SAMAL, S.P. (2025). Predictive Modelling of Surface Roughness in Grinding Operations Using Machine Learning Techniques. In: *Manufacturing Technology Journal*, Vol. 25, No. 1, pp. 14-23. Elsevier.
- [28] KARABACAK, Y. E., ÖZMEN, N. G., GÜMÜŞEL, L. (2022). Intelligent worm gearbox fault diagnosis under various working conditions using vibration, sound and thermal features. In: *Applied Acoustics*, Vol. 186, p. 108463. Elsevier.
- [29] ZHOU, W., ZHOU, Q., ZHANG, J. (2025). Speed-Load Insensitive Fault Diagnosis Method of Wind Turbine Gearbox Based on Adversarial Training. In: *Electronics*, Vol. 14, No. 4, p. 732. MDPI.
- [30] ERITENEL, T., PARKER, R. G. (2012). Three-dimensional nonlinear vibration of gear pairs. In: *Journal of sound and vibration*, Vol. 331, No. 15, pp. 3628-3648. Elsevier.
- [31] EL AMLI, A., EL YOUSFI, B., SOUALHI, A., GUILLET, F. (2025). A Novel Hybrid FEM-Dynamic Modeling Approach for Enhanced Vibration Diagnostics in a Two-Stage Spur Gearbox. In: *Energies*, Vol. 18, No. 9, p. 2176. MDPI.
- [32] FENG, Z., ZUO, M. J., HAO, R., CHU, F., EL BADAOUI, M. (2011). Gear damage assessment based on cyclic spectral analysis. In: *IEEE Transactions on Reliability*, Vol. 60, No. 1, pp. 21-32. IEEE.
- [33] FAN, Q., ZHOU, Q., WU, C., GUO, M. (2017). Gear tooth surface damage diagnosis based on analyzing the vibration signal of an individual gear tooth. In: *Advances in Mechanical Engineering*, Vol. 9, No. 6, p. 1687814017704356. Sage Publications.
- [34] GERÖCS, A., KORKA, Z. I., BLOJU, A. V., SFETCU, C. R. (2020). Appraisal of gear pitting severity by vibration signal analysis. In:

- IOP Conference Series: Materials Science and Engineering, Vol. 997, No. 1, p. 012042. IOP Publishing.
- [35] CHAARI, F., BACCAR, W., ABBES, M. S., HADDAR, M. (2008). Effect of spalling or tooth breakage on gearmesh stiffness and dynamic response of a one-stage spur gear transmission. In: *European Journal of Mechanics-A/Solids*, Vol. 27, No. 4, pp. 691-705.
- [36] HOU, J., YANG, S., LI, Q., LIU, Y. (2022). Effect of a novel tooth pitting model on mesh stiffness and vibration response of spur gears. In: *Mathematics*, Vol. 10, No. 3, p. 471. MDPI.
- [37] HAPPI, K. H. Y., KOUEJOU, B. X. T., ALUGONGO, A. A. (2023). Influence of Coexistence of Pitting and Cracking Faults on a Two-Stage Spur Gear System. In: *Vibration*, Vol. 6, No. 1, pp. 195-217. MDPI.
- [38] KIA, S. H., HENAO, H., CAPOLINO, G. A. (2014). Gear tooth surface damage fault detection using induction machine stator current space vector analysis. In: *IEEE Transactions on industrial Electronics*, Vol. 62, No. 3, pp. 1866-1878. IEEE.
- [39] BARSHIKAR, R. R., BAVISKAR, P. R. (2023). Experimental investigation for fault diagnosis of a single stage worm gearbox using response surface methodology. In: *Nigerian Journal of Technological Development*, Vol. 20, No. 2, pp. 11-22.
- [40] AHERWAR, A. (2012). An investigation on gearbox fault detection using vibration analysis techniques: A review. In: *Australian Journal of Mechanical Engineering*, Vol. 10, No. 2, pp. 169-183. Taylor & Francis.
- [41] QIU, Y., SUN, B., TAI, L. (2025). Research of Gearbox Fault Monitoring System Based on Digital Twin. In: 2025 5th International Conference on Computer, Control and Robotics (ICCCR), pp. 236-240. IEEE.
- [42] GRZESZKOWSKI, M., GÜHMANN, C., SCHOLZEN, P., LÖPENHAUS, C., NOWOISKY, S., KAPPMEYER, G. (2018). Experimental study on the pitting detection capabilities for spur gears using acoustic emission and vibration analysis methods. In: *Gear Technology*, Vol. 36, No. 2, pp. 48-57.
- [43] ZAKRAJSEK, J. J., TOWNSEND, D. P., DECKER, H. J. (1993). An analysis of gear fault detection methods as applied to pitting fatigue failure data (No. NASAE7470).
- [44] JIMÉNEZ-SANTÍN, D., CERRADA, M., SÁNCHEZ, R. V., CASSANDRO, R. (2025).

- Industry 4.0 Technologies for an Observer-Based Gearbox Fault Detection Architecture. In: 2025 IEEE International Conference on Prognostics and Health Management (ICPHM), pp. 1-7. IEEE.
- [45] ČAČO, M., KOHÁR, R., HRČEK, S., TRIBULA, R., ŠČERBA, P. (2017). Use the method of TRIZ in optimizing automated machine for ultrasonic welding. In: *Procedia engineering*, Vol. 192, pp. 80-85.
- [46] DENG, C., SHAO, Y., ZHENG, H., DU, M., YANG, Y. (2018). Research on Vibration Characteristics of Spur Gear System with Pitting Fault Considering the Elastohydrodynamic Lubrication Condition. In: 2018 18th International Conference on Control, Automation and Systems (ICCAS), pp. 1295-1299. IEEE.
- [47] ZHA, C., ZHA, S. (2022). Theoretical and Experimental Study on the Influence of Ultrasonic Vibration on Contact Friction. In: *Manufacturing Technology Journal*, Vol. 22, No. 3, pp. 367-376. Elsevier.
- [48] OSMAN, A. H., GOBRAN, M. H., MAHMOUD, F. F. (2019). Vibration signature of normal and notched tooth gear pump. In: *Eur. Sci. J*, Vol. 15, pp. 64-75.
- [49] PECHO, P., BUGAJ, M. (2018). Vibration fault detection of fuel pump using Recurrence Quantification Analysis. In: *Transportation Research Procedia*, Vol. 35, pp. 287-294. Elsevier.
- [50] SRIDHAR, V., CHANA, K. (2021). Development of a novel sensor for gear teeth wear and damage detection. In: *International Journal of Pro*gnostics and Health Management, Vol. 12, No. 3.